

In-situ Confined Synthesis of Molybdenum Oxide Decorated Nickel-Iron Alloy Nanosheets from MoO_4^{2-} intercalated Layered Double Hydroxides for Oxygen Evolution Reaction

Experimental section

Synthesis of NiFe-MoO₄²⁻ LDHs

NiFe-MoO₄²⁻ LDHs was synthesized by a hydrothermal reaction. In a typical synthesis, 0.556 g NiAc₂·4H₂O, 0.202 g Fe(NO₃)₃·9H₂O, 0.6 g urea and 0.5 g (NH₄)₆Mo₇O₂₄·4H₂O were dissolved in 50 mL of deionized water in sequence with magnetic stirring. The obtained solution was transferred into a 50mL stainless-steel Teflon-lined autoclave and heated at 160 °C for 10 h. The products were washed by deionized water and vacuum dried at 60 °C for 24 h.

Synthesis of NiFe LDHs

NiFe LDHs was synthesized by a typical synthetic method in previous work: 1.8 mmol Ni(NO₃)₂·6H₂O, 0.2mmol Fe(NO₃)₃·9H₂O and 3.5 mmol urea were dissolved in 100 mL deionized water, respectively. Then 0.025 mmol trisodium citrate (TSC) was added to above solution and stirring for 1 h. The final solution was then transferred into stainless-steel Teflon-lined autoclave and hydrothermally treated at 150 °C for 48 h. After the reaction was completed, the products were filtered, washed by deionized water and dried at 60 °C in vacuum oven.

Synthesis of CoFe-MoO₄²⁻ LDHs NS and CoFe LDHs

CoFe-MoO₄²⁻ LDHs was synthesized by the same method of NiFe-MoO₄²⁻ LDHs with the 0.556 g NiAc₂·4H₂O replaced by 0.556 g CoAc₂·4H₂O.

CoFe LDHs was synthesized by the following method: 9.3 g of Co(NO₃)₂·6H₂O and 6.5 g of Fe(NO₃)₃·9H₂O was dissolved in 40 mL of distilled water. 3.1 g of NaOH and 3.4 g of Na₂CO₃ were dissolved in another 40 mL of distilled water. The two solutions were added simultaneously into a 250 mL beaker under vigorous stirring. The mixed solution was then transferred into a teflon-lined stainless steel autoclave and heated at 80 °C for 48 h. After cooling down to room temperature, the CoFe LDHs were collected by centrifugation, washed with water, and dried at 60 °C.

Synthesis of NiFe-MoO_x NS and NiFe alloy

Both NiFe-MoO_x NS and NiFe alloy were synthesized by a calcination method. The precursor NiFe-MoO₄²⁻ LDHs and NiFe LDHs were annealed a tube furnace under Ar/H₂ (9:1) mixture atmosphere (50 sccm) with a heating rate of 5 °C/min and maintained the temperature at 500 °C for 2 h. Except the different temperature (400 °C, 600 °C, 700 °C), other conditions of those contrast samples are same with above

method. CoFe-MoO_x NS and CoFe alloy were synthesized by the same synthetic method for NiFe-MoO_x NS.

Synthesis of NiFe-MoO_x Mix

The precursor of NiFe-MoO_x Mix was a mechanical mixture of NiAc₂·4H₂O, Fe(NO₃)₃·9H₂O and (NH₄)₆Mo₇O₂₄·4H₂O with the same ratio of NiFe-MoO_x nanosheets. Then the precursor was calcined in tube furnace under the same condition of NiFe-MoO_x NS.

Electrochemical Measurements

Electrochemical measurements were performed in a three electrodes system with a electrochemical workstation (CHI 760D). For electrochemical measures of OER, 4 mg catalyst was dispersed in 1 mL ethanol. After ultrasonication for 30 min, 50 μL 5% Nafion solutions were added into the dispersion followed by another ultrasonication for 30 min. The working electrode for OER testing was prepared by dropping 100 μL above catalytic ink on a Ni foam with the apparent area 1 cm² and 10μL on a glassy carbon electrode with the surface area 0.1963 cm² (loading mass was 0.20 mg cm⁻²). All the polarization curves in this work were corrected by eliminating iR drop with respect to the ohmic resistance of the solution. The scan rate of linear sweep voltammetry (LSV) was kept at 2 mV/s. The Faradaic efficiency (ε) was calculated (see J. Am. Chem., 2014, 136 (39), 13925-13931) as follows:

$$\varepsilon = I_r / (I_d N) \quad (1)$$

Where I_d denotes the disk current, I_r denotes the ring current, and N denotes the current collection efficiency of the RRDE, which was determined using the same configuration with an IrO₂ thin-film electrode to be 0.21. To property calculate the Faradaic efficiency of the system, the disk electrode was held at a relatively small constant current of 200 uA; this current is sufficiently large to ensure an appreciable O₂ production and sufficiently small to minimized local saturation and bubble formation at the disk electrode. The TOF value was calculated from equation (2) (see *Science*, 2016, 352, 6283, 333-337):

$$TOF = \frac{j * A * \varepsilon}{4 * F * n}$$

j is obtained at *iR*-corrected overpotential = 300 mV, normalized by geometric area of GCE (0.1963 cm²); *A* is the geometric area of GCE (0.1963 cm²). *F* is the Faraday constant and ε is the Faradaic efficiency calculated from equation (2) below. *n* is the mole number of nickle and iron atoms on the electrode, calculated via the method

as followed:

$$n_{(\text{NiFe})} = \frac{m_{\text{loading}} * r(\text{NiFe}/\text{NiFe} - \text{MoO}_x)}{Mw} \quad (3)$$

where m_{loading} is the loading mass via drop-casting or spin-coating; $A(\text{BET})$ is the specific surface area; according to TGA test, $r(\text{NiFe}/\text{NiFe-MoO}_x)$ is the molar ratio of NiFe / NiFe-MoO_x, (Fe:Ni:Mo:O = 0.079:0.709:0.06:0.151); Mw is the molecular weight of NiFe-MoO_x.

Characterization.

The morphologies of synthesized materials were observed using scanning electron microscope (SEM, Hitachi, S-4800) and transmission electron microscope (TEM, FEI Tecnaï G20). The crystal structures of samples were characterized by powder X-ray diffraction (XRD, Bruker D8 Advance diffractometer, Cu K α 1). The crystalline size D was estimated by Scherrer formula as followed (4):

$$D = K\lambda / B \cos\theta$$

K is the Scherrer constant which is equal to 0.89 when B is the peak width at half peak-height of diffraction peak, λ is the wavelength of X-ray and θ is diffraction angle.

The X-ray photoelectron spectroscopy (XPS) analysis was performed by ESCALAB 250Xi X-ray photoelectron spectrometer with Mg excitation source. The binding energy was calibrated according to C (1s) neutral carbon peak at 284.8 eV. The BrunauerEmmett-Teller (BET) specific surface area and pore size distribution was probed by a nitrogen absorption-desorption method at 77 K (SSA-4200). The Raman spectra were characterized by Raman spectrometer (Labram-010) using 632 nm laser. The thermogravimetric analysis (TGA) was carried out by a STA449C instrument with a heating rate of 10 °C min⁻¹ from the room temperature to 1000 °C in air. MoO_x was changed to be MoO₃ after TGA test. So, the proportion of O in MoO_x was calculated by the figure S2b that the value of x was evaluated to be 2.49. Because of the oxidation of Ni and Fe during the process of TGA test in air, Ni and Fe were respectively transformed to NiO and Fe₂O₃. After simple calculation, the proportion of NiFe was calculated to be 61.5 wt% (molar proportion was about 78.8%) and that of MoO_x was 38.5 wt% (mole proportion was about 21.2%).

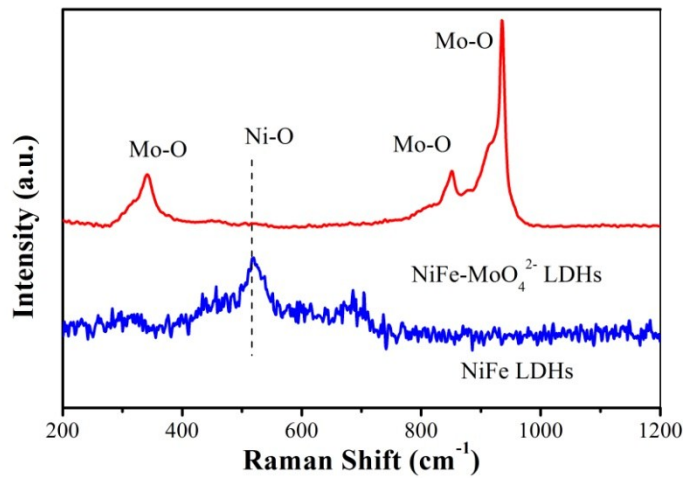
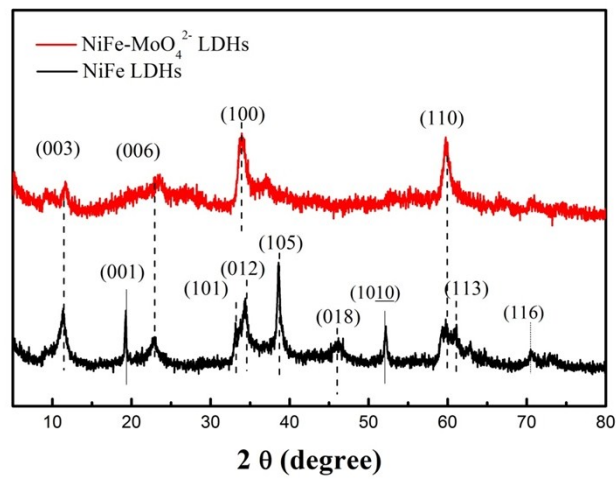


Figure S1. XRD patterns and Raman spectra of NiFe-MoO₄²⁻ LDHs and NiFe LDHs.

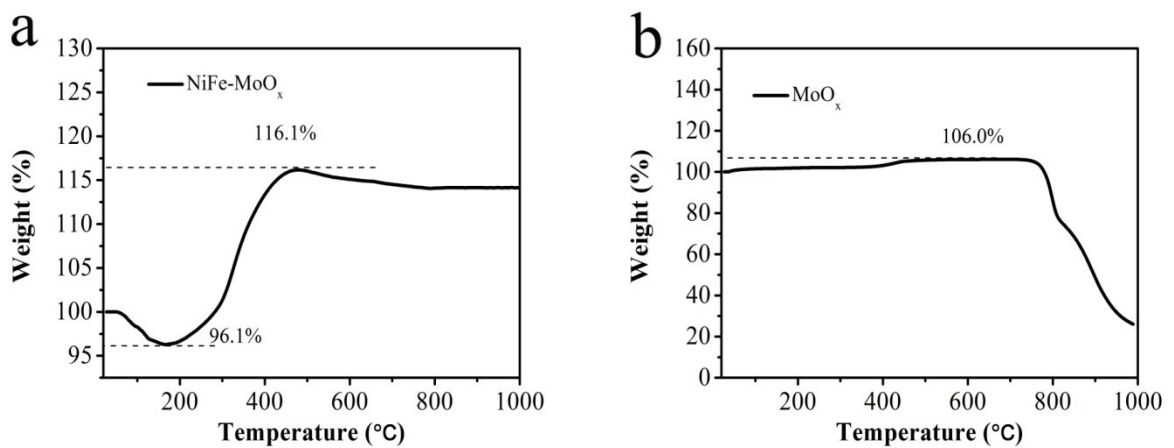


Figure S2. TGA curves of NiFe-MoO_x NS and MoO_x (For evaluating the value of x in

MoO_x, MoO_x was prepared by annealing (NH₄)₆Mo₇O₂₄·4H₂O under the same condition of NiFe-MoO_x)

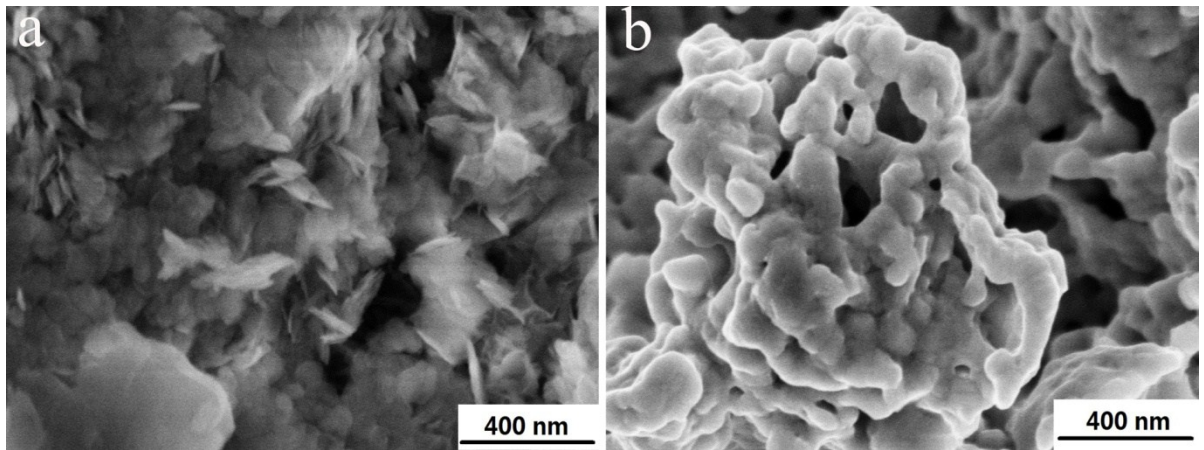


Figure S3. NiFe LDHs (a) and NiFe alloy

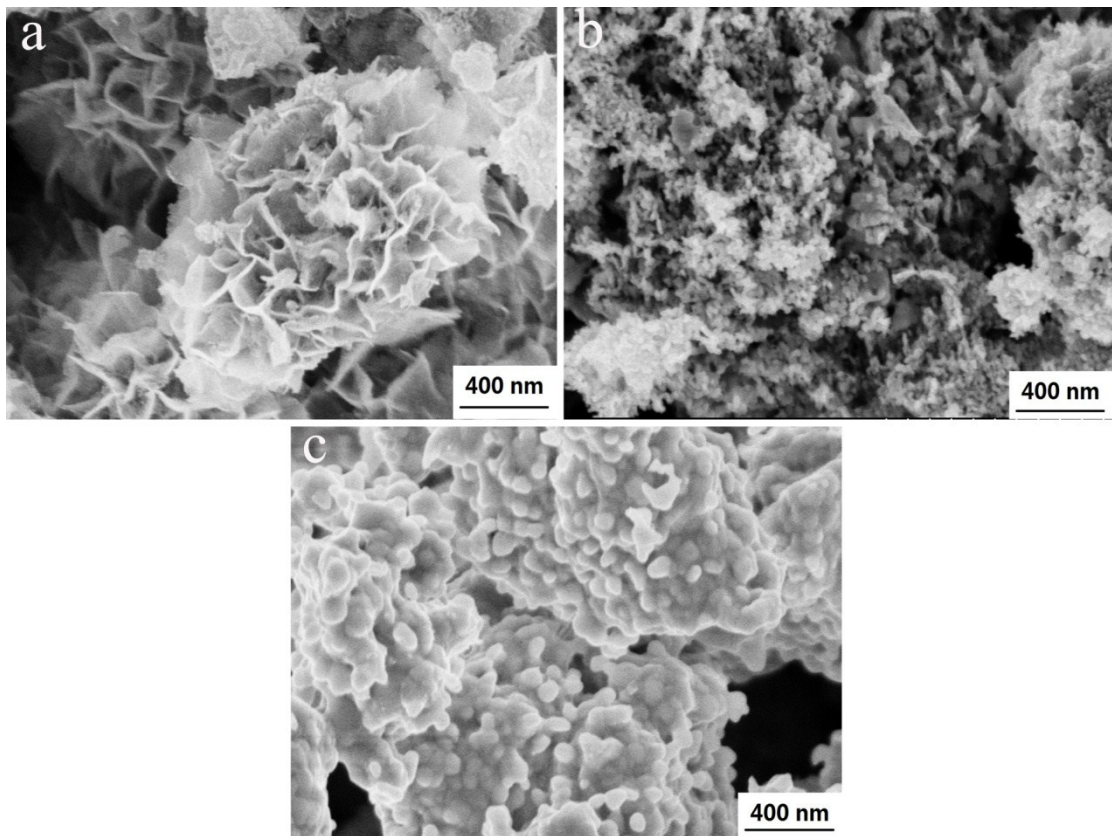


Figure S4. SEM images of (a) NiFe-MoO_x 400 (b) NiFe-MoO_x 600 (c) NiFe-MoO_x 700.

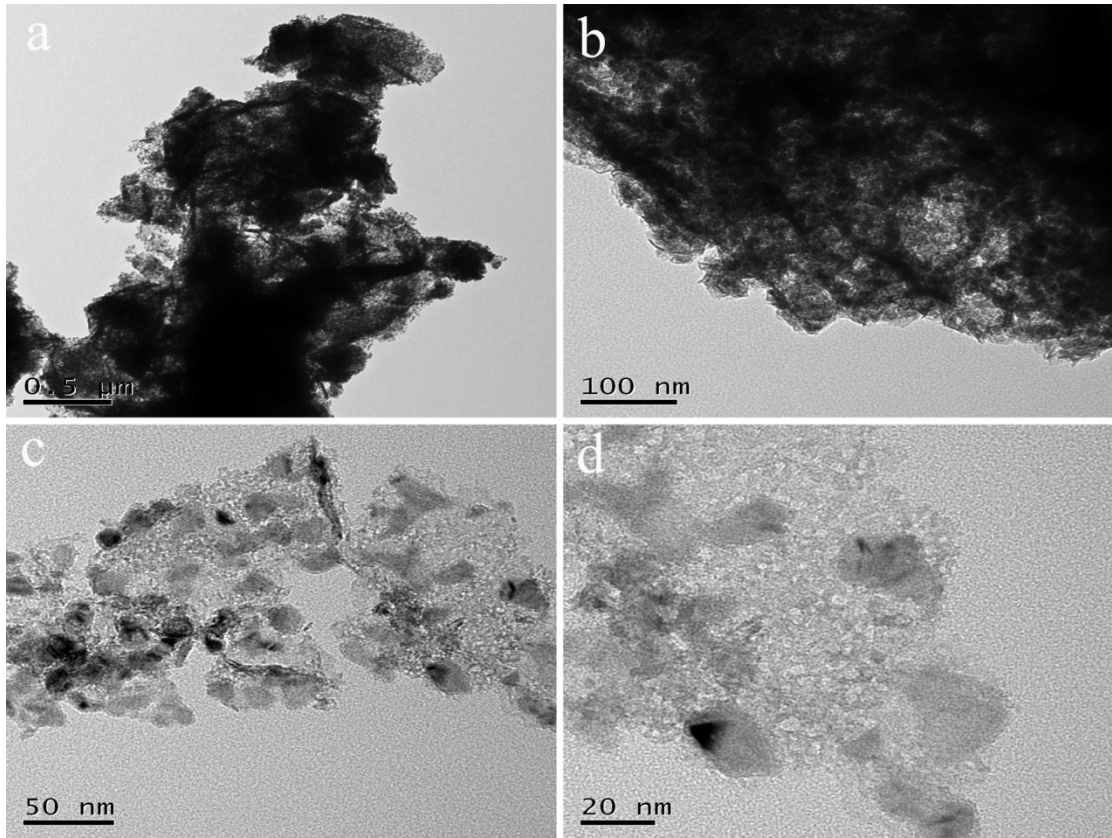


Figure S5. TEM images of NiFe-MoO_x NS.

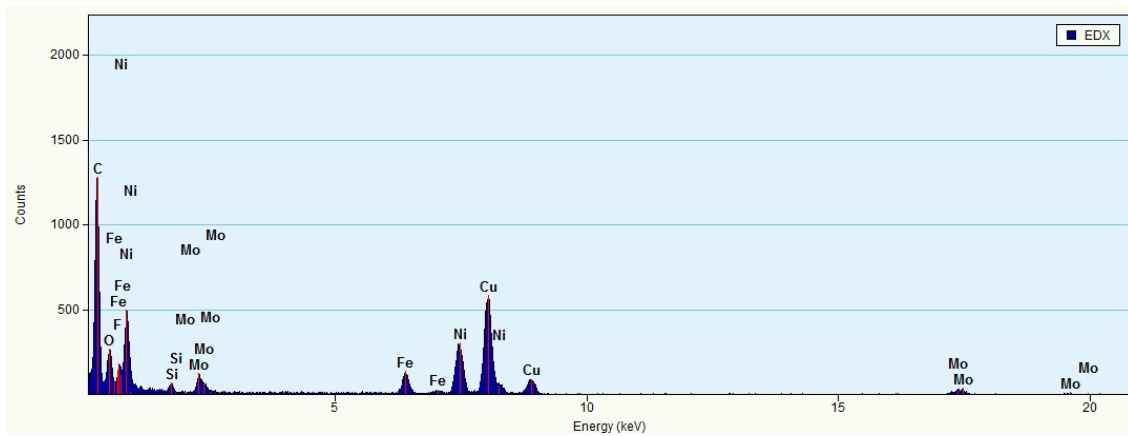


Figure S6. EDX of NiFe-MoO_x NS

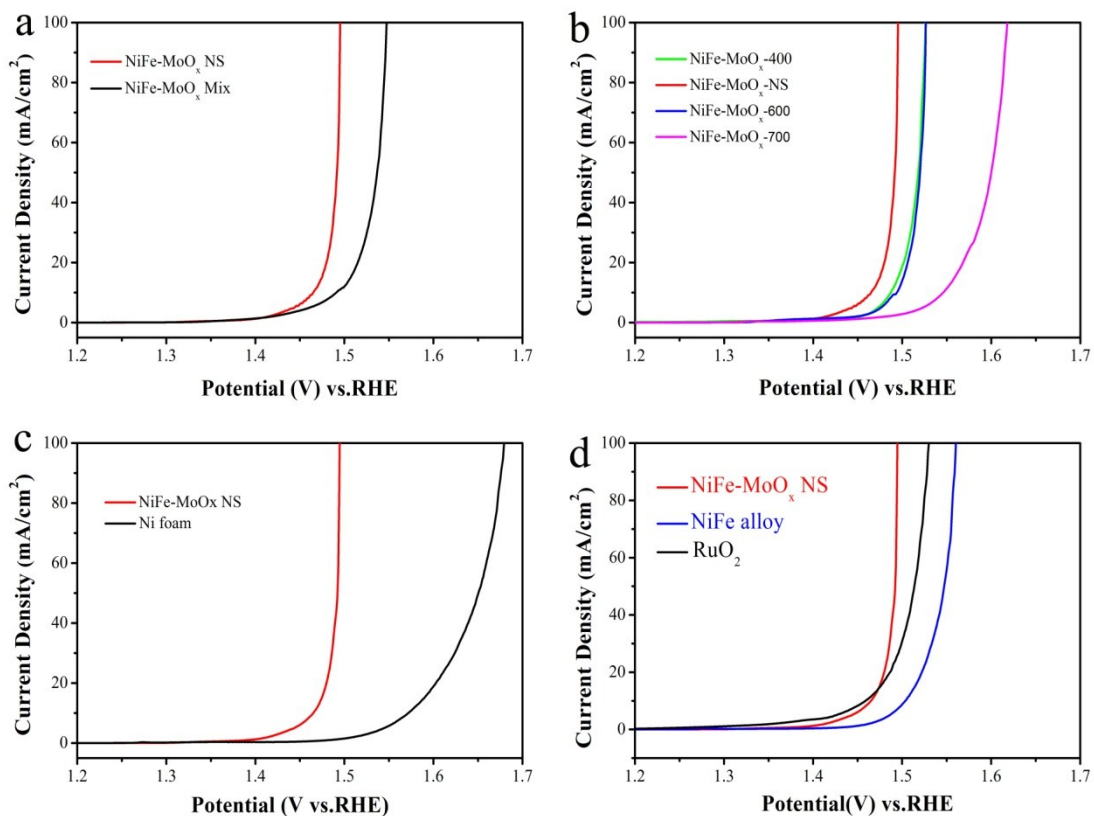


Figure S7. LSV for OER of (a) NiFe-MoO_x Mix vs. NiFe-MoO_x NS (b) NiFe-MoO_x at a series of temperature (400 °C, 600 °C and 700 °C) compared with NiFe-MoO_x NS (calcined at 500 °C) (c) Ni foam vs. NiFe-MoO_x NS and (d) NiFe-MoO_x NS and NiFe alloy. Both (a),(b),(c) and (d) were coated on Ni foam for electrochemical test.

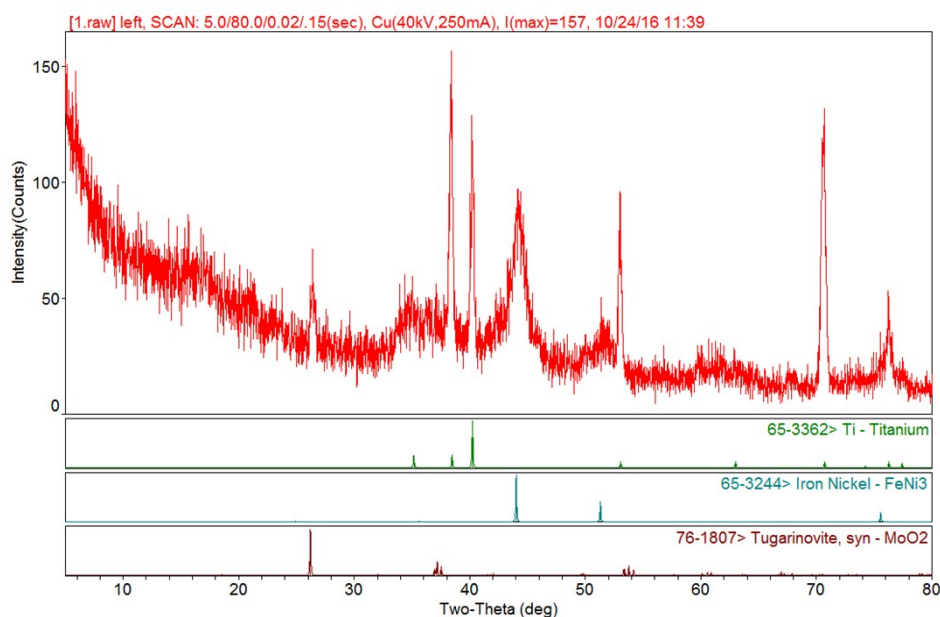


Figure S8. XRD pattern of NiFe-MoO_x NS after stability test. The NiFe-MoO_x NS powder was coated on Ti flake for electrochemical test, after that, the sample was wash by deionized water and then dry in vacuum oven in 50 °C.

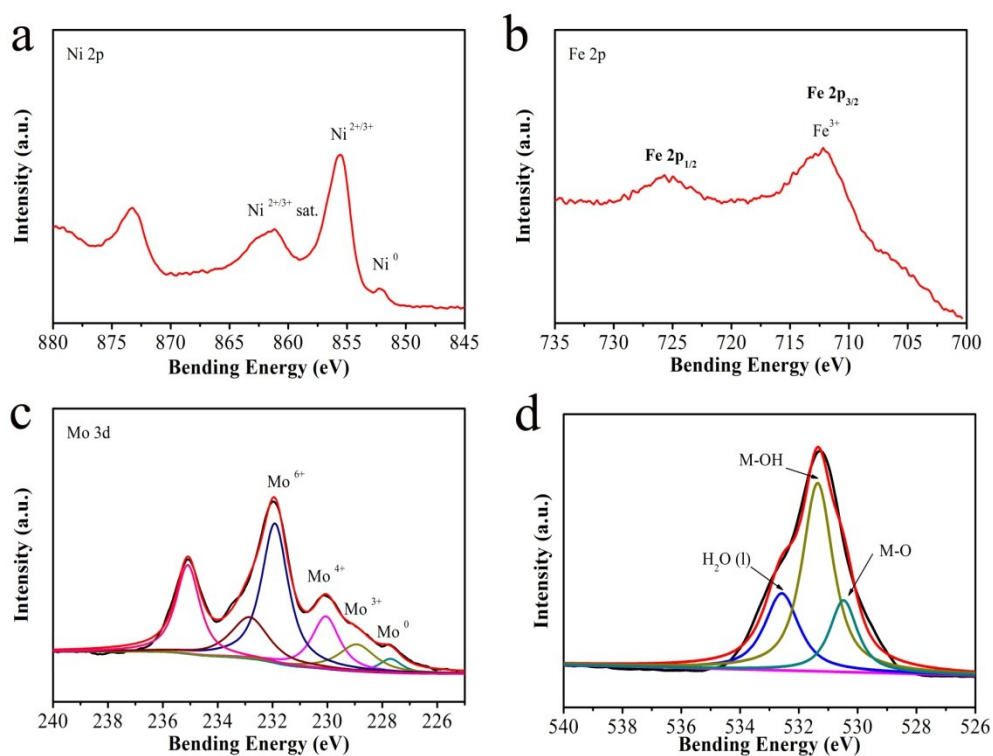


Figure S9. XPS spectra of NiFe-MoO_x NS after after stability test. (a) Ni 2p, (b) Fe 2p, (c) Mo 3d, (d) O 1s

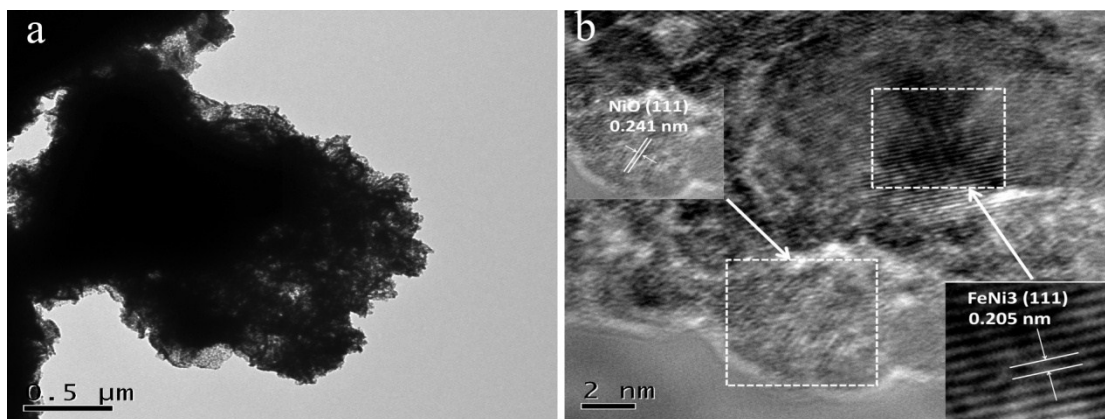


Figure S10 . TEM images of NiFe-MoO_x NS after after stability test.

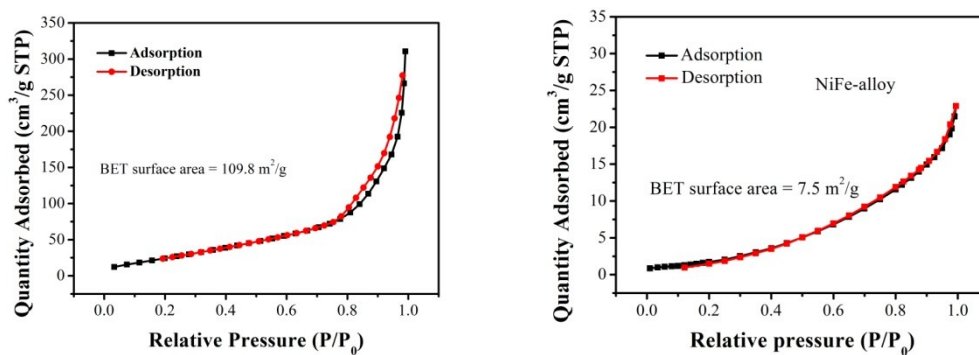


Figure S11. N₂ isotherms of NiFe-MoO_x NS and NiFe alloy

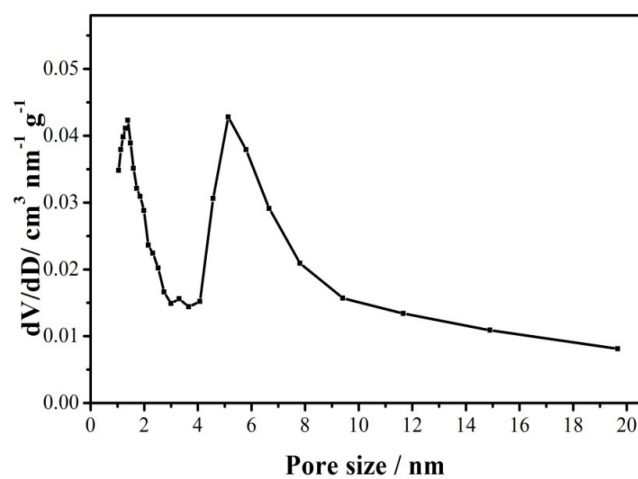


Figure S12. Pore size distribution of NiFe-MoO_x NS.

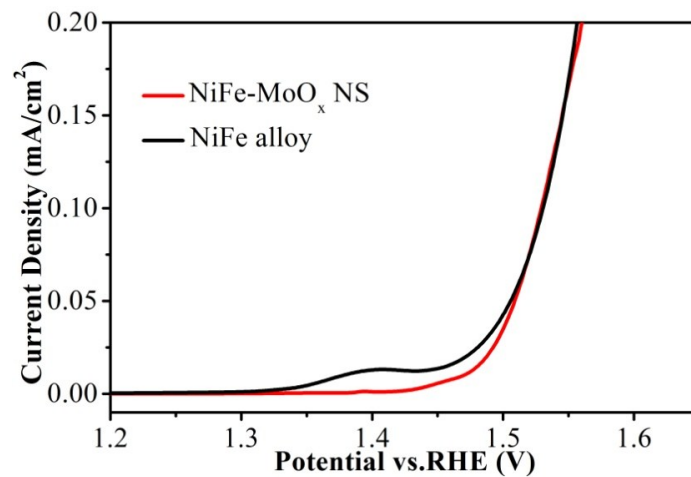


Figure S13. LSV for OER of NiFe-MoO_x NS and NiFe alloy normalized by BET surface (in Figure S9).

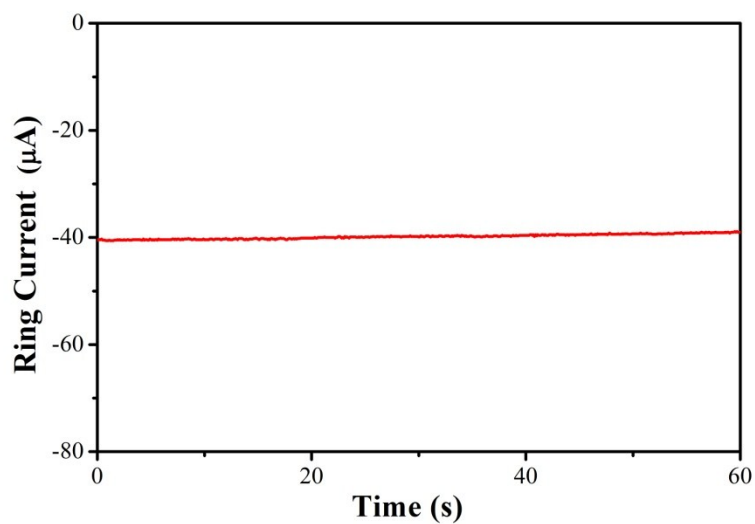


Figure S14. The Faradaic efficiency curve of Co₃FeN_x for OER.

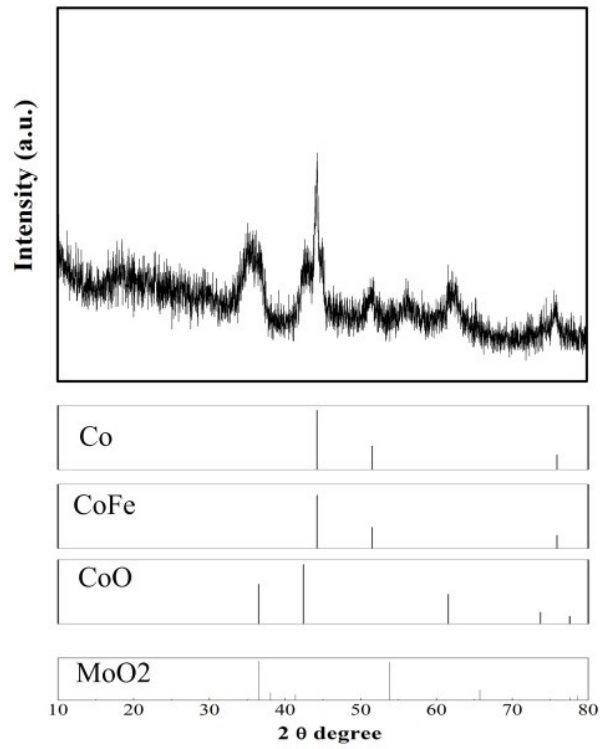


Figure S15. XRD pattern of CoFe-MoO_x NS.

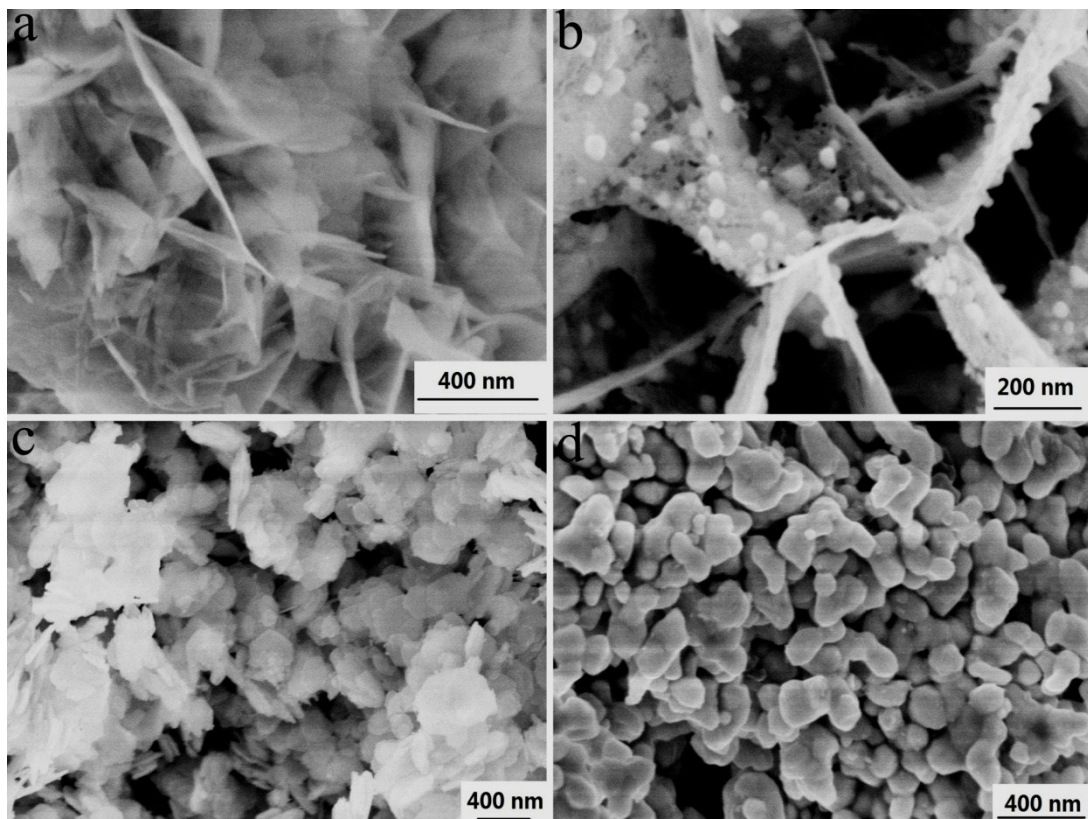


Figure S16. SEM images of (a) CoFe-MoO₄²⁻ LDHs (b) CoFe-MoO_x NS (c) CoFe LDHs and (d) CoFe alloy.

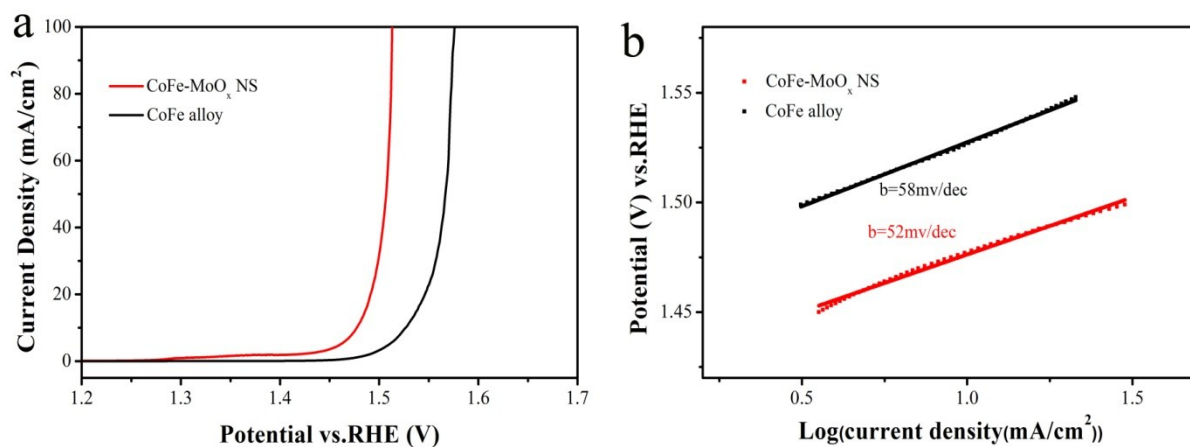


Figure S17. (a) LSV for OER of CoFe-MoO_x NS and CoFe alloy (b) Tafel slope of CoFe-MoO_x NS and CoFe alloy.

Table S1. Comparison of OER activity of the NiFeMoO_x NS with recently reported catalyst

Electrocatalyst	Electrolyte	Current density (mA/cm ²)	Overpotential at 10 mA/cm ² (vs. RHE) (mV)	Tafel slope (mV/dec)	Reference
NiFe-MoO _x NS	1 M KOH	10	276	55	This work
NiFe-LDH nanosheets	1 M KOH	10	302	40	S4
NiFeMn- LDHs	1 M KOH	10	250	47	S5
NiFe/NC	1 M KOH	10	320	45	S6
NiFe-LDH/CNT	1 M KOH	10	228	35	S7
NiFe-DAT	1 M NaOH	100	300	--	S8
Ni _{0.75} Fe _{0.25} OOH	1 M KOH	10	258	--	S9

FeNi-rGO LDH	1 M KOH	10	208	38	S10
NiFe-MMO/CNT	1 M KOH	10	220	45	S11

References:

- S1.** N. Han, F. Zhao and Y. Li, *J.mater.chem.a*, 2015, **3**, 16348-16353.
- S2.** Y. Han, Z. H. Liu, Z. Yang, Z. Wang, X. Tang, T. Wang, L. Fan and K. Ooi, *Chemistry of Materials*, 2008, **20**, 360-363.
- S3.** D. Du, W. Yue, Y. Ren and X. Yang, *Journal of Materials Science*, 2014, **49**, 8031-8039.
- S4.** F. Song and X. Hu, *Nature Communications*, 2014, **5**, 4477-4477.
- S5.** Z. Lu, L. Qian, Y. Tian, Y. Li, X. Sun and X. Duan, *Chemical Communications*, 2015, **52**, 908-911.
- S6.** X. Zhang, H. Xu, X. Li, Y. Li, T. Yang and Y. Liang, *Acs Catalysis*, **2016**, *6* (2), pp 580–588
- S7.** M. Gong, Y. Li, H. Wang, Y. Liang, J. Z. Wu, J. Zhou, J. Wang, T. Regier, F. Wei and H. Dai, *Journal of the American Chemical Society*, 2013, **135**, 8452-8455.
- S8.** T. T. H. Hoang and A. A. Gewirth, *ACS Catalysis*, **2016**, *6* (2), pp 1159–1164
- S9.** M. S. Burke, S. Zou, L. J. Enman, J. E. Kellon, C. A. Gabor, E. Pledger and S. W. Boettcher, *Journal of Physical Chemistry Letters*, **2015**, *6* (18), pp 3737–3742
- S10.** X. Long, J. Li, S. Xiao, K. Yan, Z. Wang, H. Chen and S. Yang, *Angewandte Chemie International Edition in English*, 2014, **53**, 7584-7588.
- S11.** Y. Li, H. He, W. Fu, C. Mu, X. Z. Tang, Z. Liu, D. Chi and X. Hu, *Chemical Communications*, 2015, **52**, 1439-1442.